Colloids and Surfaces B: Biointerfaces 217 (2022) 112666

Contents lists available at ScienceDirect

Colloids and Surfaces B: Biointerfaces

journal homepage: www.elsevier.com/locate/colsurfb

Reduction of calcified plaque volume in ex vivo pericardial tissue, with nanobubbles

A. Li [a], Y. Li [b], S. Qiu [b], P.M. Patel [c], Z. Chen [b], J.C. Earthman [a,b,*]

[a] Department of Materials Science and Engineering, University of California, Irvine, CA 92697, USA
[b] Department of Biomedical Engineering, University of California, Irvine, CA 92697, USA
[c] Department of Medicine, University of California, Irvine, CA 92697, USA

ARTICLE INFO

Keywords:
Atherosclerotic plaque
Nanobubbles
Ringer's solution
Intravascular optical coherence tomography
Induced plaque reduction

ABSTRACT

The present research investigated the effect of nanobubbles in Ringer's solution on calcified plaque within ex vivo coronary and peripheral artery tissue. The goal of the work was to determine whether nanobubbles generated using an alternating magnetic field (AMF) system can reproducibly reduce the size of plaque obstructions in ex vivo pericardial tissue specimens compared to that in an untreated control. Nanoparticle tracking analysis (NTA) measurements were used to first confirm that AMF can produce nanobubbles in Ringer's solution as well as it does in water. Experiments were performed in which ex vivo human coronary artery and peripheral artery tissues containing plaque were exposed to Ringer's solution with and without the presence of AMF generated nanobubbles. Measurements on intravascular optical coherence tomography (IVOCT) images consistently indicated that plaque volume is significantly reduced in the presence of nanobubbles. A theory of induced dissolution by nanobubble/nanoparticle cluster formation provides a causal explanation for the observed reductions in plaque size.

1. Introduction

Atherosclerosis is a chronic inflammatory disease that leads to most heart attacks and strokes and was the root cause of approximately 32 % of global mortalities in recent years [1]. Unstable atherosclerotic plaque causes coronary artery disease and peripheral artery disease. Furthermore, plaque rupture or erosion causes myocardial infarctions and strokes [2]. Some biochemistry approaches for preventing or treating atherosclerosis by applying vaccines, nano-agents, etc., have shown some promise but still must overcome formidable challenges to be considered safe and effective [3,4].

Observations of nanobubbles (NBs) on hydrophobic surfaces were first reported in 2001 [5]. Later, several reports began to appear on the observation and properties of NBs in bulk solutions that exhibit extraordinary stability [6,7]. Further research has indicated that the long-term stability of NBs is associated with an electrically charged liquid–gas interface resulting in a relatively high zeta potential [7,8]. Recently, Satpute and Earthman [9] showed how NB stability can be attributed to the concentration of hydroxyl ions on the surface during shrinkage of microbubbles that ultimately produce repulsive forces that can balance the surface tension once the bubble size reaches the nanoscale. Unlike previous attempts, this first-principles theory for nanobubble stability requires no unconfirmed assumptions or conditions.

Nanobubbles have been investigated for water treatment [10–12] and surface antifouling treatment [13–15] because of their extremely small size and ability to bind to nanoparticles [12]. Recent studies on in vivo applications of NBs, are focusing on utilizing them carriers for ultrasound contrast agents [16–18] and ultrasound-triggered drug delivery [19–22], taking advantage of their slow decay rate, high intercellular permeability, and ultrasonic properties.

Uchida and coworkers have shown that nanoparticles in saline and wastewater bind to nanobubbles using a freeze-fracture replica method in conjunction with transmission electron microscopy (TEM) [12]. Quach and colleagues [23] recently reported evidence that nanobubbles bind to calcium carbonate nanoparticles at the solubility limit of $CaCO_3$ in neutral water. They also showed how this binding process could explain observed dissolution of compounds that deposited on walls of service water piping. This binding process was attributed to the fact that NBs have a significantly negative zeta potential [12] and, because they provide a small but widely dispersed gas-water interface, they offer a favorable binding site to hydrophobic nanoparticles. It follows that NBs

* Corresponding author at: Department of Materials Science and Engineering, University of California, Irvine, CA 92697, USA.
E-mail address: earthman@uci.edu (J.C. Earthman).

https://doi.org/10.1016/j.colsurfb.2022.112666
Received 23 February 2022; Received in revised form 22 June 2022; Accepted 25 June 2022
Available online 27 June 2022

could also bind to nanoparticles of calcium compounds in other aqueous solutions including intravenous fluid.

Atherosclerotic calcification involves complex signaling pathways and bone-like genetic processes [24]. During atherosclerosis, calcification can be initiated by vascular smooth muscle cells within the arterial wall that obtain an osteoblast-like phenotype and release hydroxyapatite (HA), $Ca_5(PO_4)_3OH$ [25]. Macrophage apoptosis is another prominent source of calcification within atherosclerotic plaque [26]. It is possible that NBs can bind to unstable $Ca_5(PO_4)_3OH$ nanoparticles (embryos) that would keep these embryos from dissolving back into solution. Therefore, it follows that formation of NB/nanoparticle clusters could then lower the concentration of dissolved $CaPO_4$ to levels well below its solubility limit. This process is depicted schematically in Fig. 1. It is reasonable to assume that $Ca_5(PO_4)_3OH$ in plaque could start to dissolve as the concentration of $CaPO_4$ in the surrounding medium falls below the solubility limit. Accordingly, the central hypothesis of the present work is that the stability of atherosclerotic calcification may be affected by the administration of sufficient numbers of nanobubbles. This research consisted of experiments that were designed to test this hypothesis with ex vivo tissue samples.

2. Methods

2.1. Nano-bubble generation and measurement

An alternating magnetic field (AMF) NB generating system was used in the present work [23]. Ringer's solution circulated through the AMF NB generator at a rate of 270 mL/min and pressure of 13.8 kPa. The composition of the Ringer's solution (Fisher Scientific, Fair Lawn, NJ) used in the present work in g/L is 9.2 sodium chloride, 1.5 sodium bicarbonate, 0.4 potassium chloride, 0.2 calcium chloride in water. We note that while some calcium is present in Ringer's solution, this solution used in the present work does not also contain phosphate ions.

Unaltered and AMF treated Ringer's solution samples were analyzed using a NanoSight NS300 (Malvern Panalytical Ltd, Malvern, UK) for NB/nanoparticle size distribution and relative scattering intensity. The size calculated by NanoSight is the equivalent spherical hydrodynamic diameter of the objects scattering light. The relative light scattering intensity is directly measured by a CCD camera, and it is primarily related to index of refraction and size of the objects (particles or bubbles) in the solution. According to Rayleigh scattering theory for objects smaller than the wavelength of the incident light [27], light scattering intensity, I, in water is positively correlated with the relative index of refraction, n, of the nano-objects as:

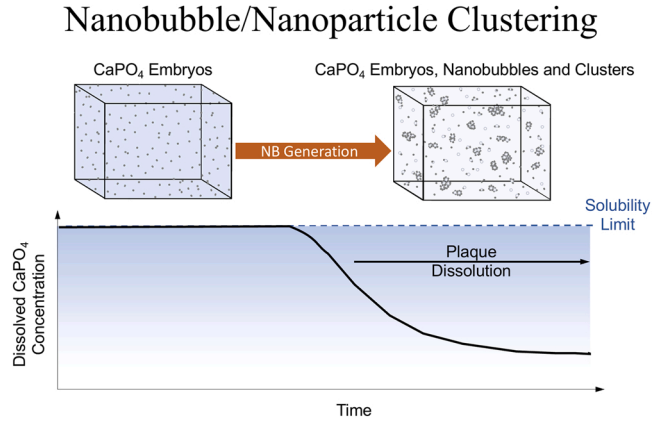

Fig. 1. Schematic of the effective reduction in dissolved calcium phosphate concentration by the clustering of $CaPO_4$ nanoparticles (embryos) with nanobubbles. As the concentration of dissolved $CaPO_4$ drops below the solubility limit, dissolution of $Ca_5(PO_4)_3OH$ in calcified plaque could then be induced.

$$I \propto \left(\frac{n^2-1}{n^2+2}\right)^2 \quad (1)$$

The relative refractive index is given by:

$$n = \frac{n_o}{n_w} \quad (2)$$

where n_o is the index of refraction of the nanoscale object and n_w is the refractive index of water. Thus, it should be possible to distinguish nanoscale objects of similar size that have different relative indices of refraction by comparing the scattered light intensity they exhibit. The index of refraction for water is 1.33. Bunkin and coworkers [28] reported a refractive index for nanobubbles of about 1.26, which is somewhat higher than that for a gas ($n_g = 1.0$). However, it is possible that the relatively high concentration of ions on the surface of nanobubbles could be responsible for the greater than expected refractive index of nanobubbles observed [9]. The resulting value of n for nanobubbles in water is then about 0.95. By comparison, the index of refraction for calcium phosphate is approximately 1.63 and, therefore, its value of n in water is 1.23. We note that the value of n for other salts such as NaCl would also be in this range. Compared to that for salt nanoparticles in Ringer's solution, NBs of similar size should then correspond to a substantially lower light scattering intensity according to Eq. (1). Nanoparticle Tracking Analysis (NTA) software that accompanies the NanoSight NS300 instrument was used to determine relative light scattering intensity for each sample analyzed. Each sample run in this instrument was conducted for 60 s.

The Z test was used to assess the number of duplicate Nanosight runs necessary to achieve representative data distributions for nanobubbles and nanoparticles. An approach approximated to power analysis was used to assess this number of duplicate NTA runs (N). In this approach, the averages and standard deviations of all possibilities from combining up to a total of 10 runs were calculated. Two proportion Z test was used to calculate the Z score for the one-to-one combinations of all these possibilities. It was found that when $N = 5$, approximately 90 % of these combinations have no significant difference, at a confidence level at 95 % ($Z < 1.96$). We note that a rate of 80 % is the power typically accepted as sufficient in power analyses. Thus, results from averaging five duplicate runs in NTA were considered sufficient in the present work to be considered statistically significant.

2.2. Experimental system

A circular flow test system (CFTS) was used in the present that consists of a pump, three-way valve, AMF system, pressure gauges, flow meters, reservoir with immersion heater, and pinch valve for controlling flow rate. A schematic of the present CFTS is shown in Fig. 2.

2.3. Tissue sample preparation

Fresh coronary arteries and peripheral arteries were obtained from cadavers, rinsed with Ringer's solution and frozen in a − 19 °C freezer. Coronary artery samples were supplied by Willed Body Program at the University of California, Irvine, while peripheral artery samples were supplied by Medtronic Inc. All methods were carried out in accordance with the University of California, Irvine (UCI) Institutional Review Board (IRB) and the Institutional Biosafety Committee (IBC). All experimental protocols were approved by the UCI IBC under protocol #2016–1570.

2.4. Nanobubble exposure experiments

The Ringer's solution was pumped through the CFTS in bypass mode (no NBs) until its temperature reached 37 °C. Each artery sample was mounted at the side stream outlet to the reservoir (see Fig. 2). A side

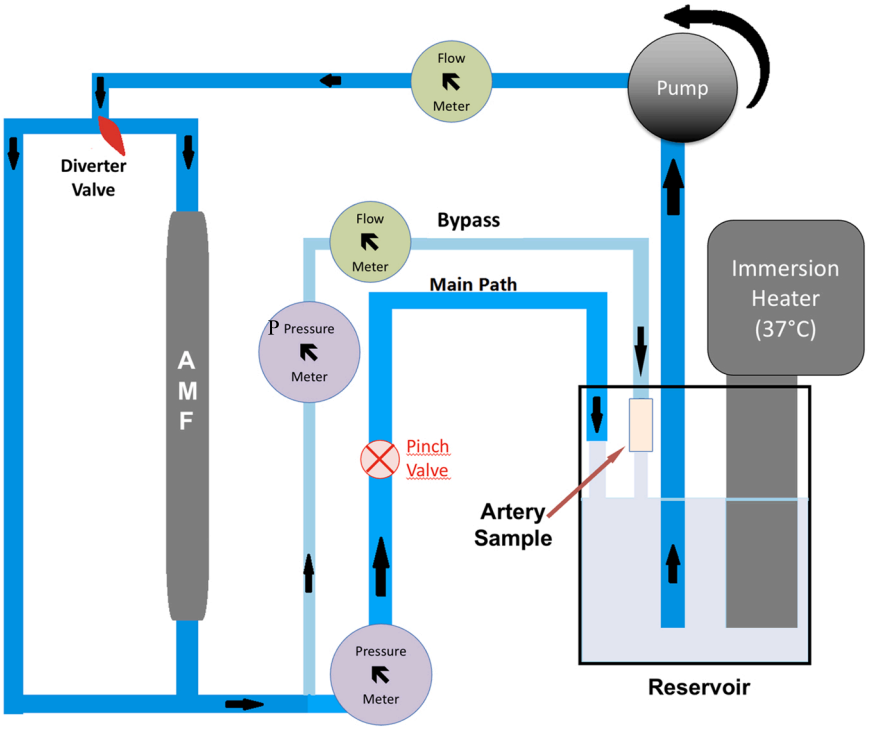

Fig. 2. Schematic of the present circular flow test system (CFTS).

stream was used to reduce the flow rate through the artery sample to be consistent with physiological flow rates. For test conditions, nanobubbles were added to the system by switching the diverter valve shown in Fig. 2. Another valve in main flow path was used to adjust the flow pressure from 10.0 kPa to 10.7 kPa with a fixed flow rate of ~240 mL/min. Exposure to flowing Ringer's solution for most samples was performed for 4 h. Exceptions were samples S6A and S6B that were treated for 6 h in total, and intravascular optical coherence tomography (IVOCT) was performed every 2 h during interruptions of the experiments.

2.5. Intravascular optical coherence tomography

IVOCT was performed before and after treatment experiments on the present ex vivo samples. The IVOCT system was developed at the Beckman Laser Institute, at the University of California, Irvine [29]. This system uses a laser with a 1310 nm center wavelength and has an axial resolution of 12 μm and a transverse resolution of 30 μm. The pullback speed of the probe was set to 3 mm/s, with an acquisition rate of 50 frames per second. Thus, the corresponding distance between two frames is 60 μm. This method is ideal for arterial samples since the probe can image plaque over the entire surrounding artery wall at each frame position. IVOCT images of the entire arterial tissue sample were obtained before and after exposure to the Ringer's solution in the CFTS for three hours. Once all of the IVOCT images for a given sample were acquired, plaques in the images were located and tracked in all of the frames in which each plaque was observed, neighboring plaques and other morphological features. There are primarily three types of atherosclerotic plaques: fibrous, lipid and calcified types, where the calcified type of plaque has the lowest backscattered light coefficient ($\mu b_{Calcium} = 4.9 \pm 1.5\ mm^{-1}$, compared to $\mu b_{Fibrous} = 18.6 \pm 6.4\ mm^{-1}$, $\mu b_{Lipid} = 28.1 \pm 8.9\ mm^{-1}$) in OCT [30].

Backscattering is positively related to the grayscale on the IVOCT images. The lowest backscattering results for calcium containing plaques. Since other surrounding soft tissues in the arterial wall give rise to relatively high levels of backscattering, the calcified plaques tend to give rise to more contrast with the surrounding tissues compared to the other plaque types. If not stated in the results, the default plaque type measured using IVOCT in the present work was calcified plaque.

Six heart coronary artery samples (CAS) and two peripheral superficial femoral artery samples (PAS) were treated in the CFTS with Ringer's solution, with or without NBs. One or two plaques were identified using IVOCT in each sample except in the case of sample CAS 1, for which three plaques were identified. The volume of each plaque was measured over multiple frames before and after the treatment using ImageJ image analysis software (National Institutes of Health, Bethesda, Maryland, USA). Test specimens CAS 1, CAS 2, CAS 5, and PAS 1 were exposed to Ringer's solution containing nanobubbles (NBs), while control samples CAS 3, CAS 4, and CAS 6 were exposed to unaltered Ringer's solution.

3. Results and discussion

3.1. Nanoparticle/nanobubble measurements

Fig. 3 shows NTA data for Ringer's solution treated in the present CFTS both with and without the addition of NBs, as 3D plots of nanoscale object concentration as a function of size and light scattering intensity. In the test groups (NB Treated), two distinct peaks with comparable object concentration and size but different light scattering intensity were observed. For the control replicates, there is only one prominent peak shown in Fig. 3 (Untreated).

There are both calcium ions and bicarbonate ions in the present Ringer's solution (Table 1). For the present conditions of 37 °C, 1 bar of air pressure and a pH of 7.3, the solubility of calcium carbonate is approximately 2 mmol/L [25]. This concentration is close to that for calcium ions in of Ringer's solution. Thus, it follows that calcium carbonate embryo nanoparticles were forming and dissolving in the liquid phase during the present experiments. The peaks in Fig. 3 with higher light scattering intensity for the test groups could be produced by nanoparticle clusters assuming that the embryo nanoparticle becomes stable once it binds to a NB, which reduces its surface energy. The peaks at lower light scattering intensity in the test replicates have smaller average size compared to the peaks at higher light intensity. It follows

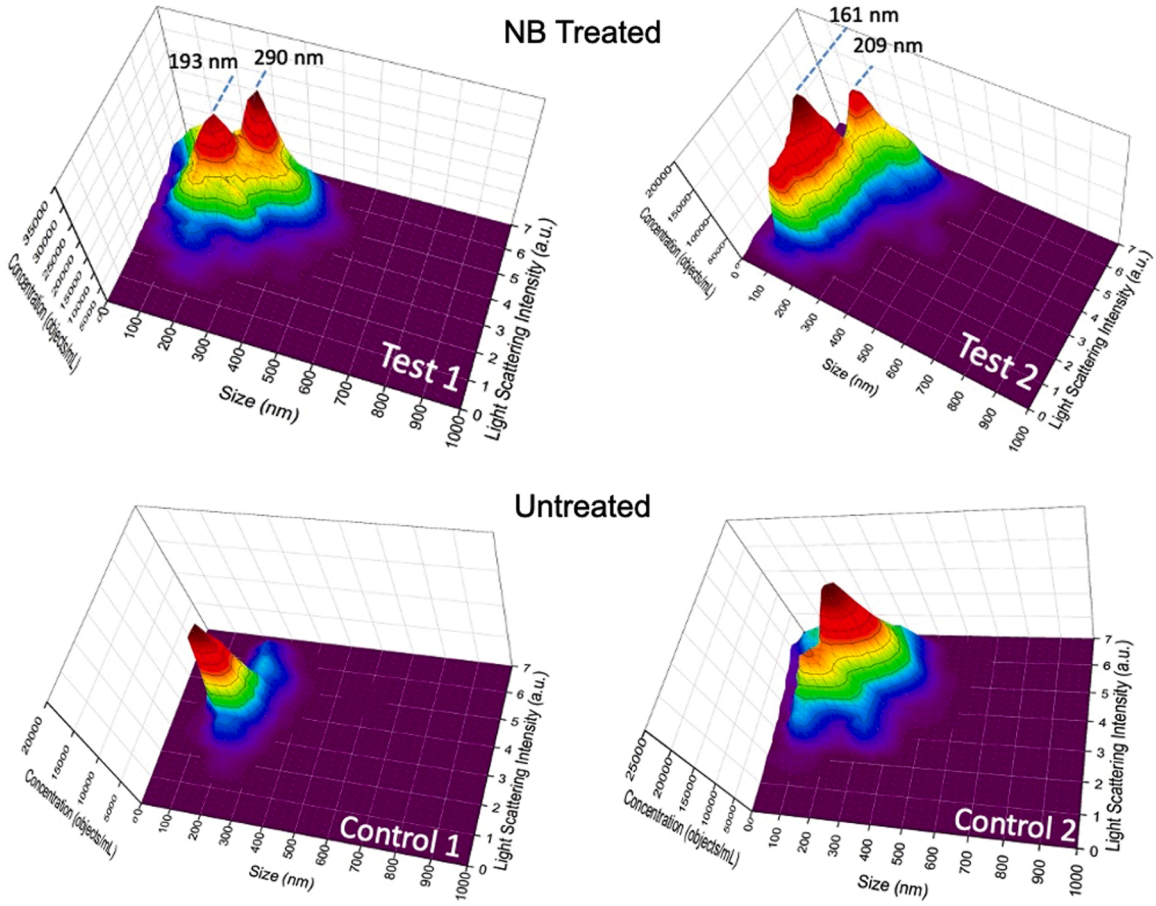

Fig. 3. Replicate sets of NTA data plotted as size and relative light intensity (arbitrary units) plotted as a function of object concentration for Ringer's solution treated with NBs (Test 1 and 2), and that without NB addition (Control 1 and 2). The results were obtained from four separate solution samples that were circulated through the present CFTS system for 3 h. Each replicate was run five times in the NanoSight NS300 and the results were averaged.

Table 1
Composition of the Ringer's solution used in the present research (g/L).

Sodium Chloride	Sodium Bicarbonate	Potassium Chloride	Calcium Chloride
9.2	1.5	0.4	0.2

that the lower intensity peaks should correspond to light scattering by NBs, that have significantly lower index of refraction compared to calcium carbonate nanoparticles. These results are consistent with the assertion that NBs can be generated using an alternating magnetic field [23].

NanoSight NTA has also been applied to the Ringer's solution samples collected after testing ex vivo tissue samples CAS 1 (Test) and CAS 3 (Control) in the present CFTS. Three dimensional plots of concentration

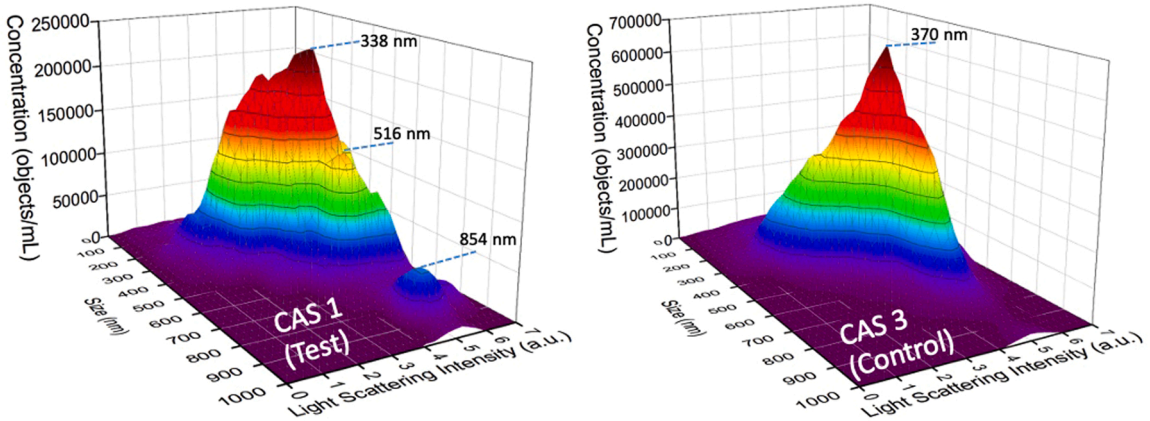

Fig. 4. NTA data plotted as size versus relative light intensity and object concentration for Ringer's solution after treatment in the presence of *ex vivo* coronary artery samples CAS 1 (Test with NB addition) and CAS 3 (Control without NB addition). Each sample was run 10 times in the NanoSight NS300 and the results were averaged.

versus size and relative intensity are shown in Fig. 4. For these plots, each sample was run 10 times in the NanoSight NS300 and the results were averaged. Fig. 4 indicates that the overall concentration of nanoscale objects in the solution for CAS 1 is less than 50 % of the concentration in the control (CAS 3). This lower overall concentration with the addition of nanobubbles can be explained by the formation of NB-nanoparticle clusters that can substantially reduce the total number of both individual NBs and nanoparticles in solution.

Ex vivo tissue sample CAS 1 exhibited two concentration peaks for two different relative intensities for sizes below about 340 nm as shown in Fig. 4. The concentration peak at higher scattering intensity should correspond to nanoparticles while the concentration peak at lower scattering intensity should correspond to NBs. For CAS 3, control with no NBs, single peak for the nanoparticles present is present at a size of about 370 nm (Fig. 4). The peaks corresponding to NBs in test samples 1 and 2 shown in Fig. 3 were observed at object sizes of 193 nm and 161 nm, respectively. We then take the average of these measurements (177 nm) as an estimate of mean diameter for the NBs. The minimum diameters of a single NB–single nanoparticle cluster and, based on the apparent higher concentration of nanoparticles than NBs, a cluster of nanoparticles bound to a single NB can be approximated by the following:

$$d_{\text{minimum cluster}} = d_{\text{NB}} + d_{\text{nanoparticle}} = 177\ \text{nm} + 370\ \text{nm} = 547\ \text{nm} \tag{3}$$

$$d_{\text{single NB cluster}} = d_{\text{NB}} + 2\,d_{\text{nanoparticle}} = 917\ \text{nm} \tag{4}$$

where d is the corresponding diameter. The assumptions made here are that the shape of nanoparticles, as well as that for the NBs, is roughly spherical and clusters form between one NB and either one or multiple nanoparticles. We note that the size of 516 nm corresponding to a concentration peak for CAS 1 is only slightly smaller than the estimate for a small dual object cluster structure predicted by Eq. (1). Further, the peak corresponding to a size of 854 nm agrees reasonably well with the estimate of 917 nm given by Eq. (2). We note that Eqs. (3) and (4) predict an upper limit for the measured hydrodynamic diameter of these clusters due to asymmetry and spaces between nanoparticles. By comparison, there are no peaks larger than the single peak at about 370 nm in the plots for the untreated control (CAS 3) in Fig. 4. In sum, the NTA evidence in these figures clearly supports the formation of clusters by NB/nanoparticle binding.

3.2. Plaque measurements

IVOCT images are shown in Fig. 5 of a calcified plaque (a), and a lipid plaque (b) that were discovered in specimens CAS 3 and CAS 2, respectively. Both plaques are discernible because the calcified plaque corresponds to mostly lower (darker) grayscale value compared to the surrounding tissue while that for the plaque with a lipid character corresponds to predominantly higher (lighter) grayscale value compared to the surrounding tissue. However, both light and dark regions can be seen within both types of plaques in Fig. 5.

Representative IVOCT images of plaque sample CAS 1 III taken before and after NB treatment are shown in Fig. 6 at approximately the same location. A reduction in volume can be seen by comparing these images. We note that several stacked images for each plaque were used to measure its entire volume as opposed to just the one image (slice) shown here for each.

IVOCT results plotted in Fig. 7 indicate that plaque volume in the coronary decreased by approximately 36 % on average with a NB treatment of four hours (CAS. 1 I, CAS 1 II CAS III, CAS 2 and CAS 5). By comparison, control group CAS 3, CAS 4 I, CAS 4 II, CAS 6 I and CAS 6 II exhibited a mean plaque reduction of only about 7 % after four hours exposure to untreated Ringer's solution with the same flow rate for four hours. We note that the plaque in CAS 2 appeared to have a more lipid character compared to the other plaques which were the calcified type. Despite this appearance, it also exhibited a volume reduction that was greater than those observed for the control specimens.

A Student's T-test was performed to determine the difference between the NB treated and control groups shown in Fig. 7. The resulting p value for this T-Test is 0.0027, which is well below the often used criterion of $p < 0.05$ to indicate a statistically significant difference in mean values. Thus, the presence of NBs consistently and significantly led to a greater reduction in plaque volume compared to Ringer's solution without NBs.

We note that a small reduction in plaque volume in control experiments was expected since Ringer's solution does not contain phosphate which is typically a component of calcified plaque. Thus, some dissolution of $CaPO_4$ in each specimen would occur until the solubility limit of $CaPO_4$ is reached in the surrounding liquid, which is very low ($\sim 9 \times 10^{-8}$ mol/L).

IVOCT results for two superficial femoral arteries, PAS 1 exposed to Ringer's solution containing NBs and PAS 2 exposed only to control solution, are illustrated in Fig. 8. The plaque size measurement before and after these experiments indicated that both plaques had much higher volume deduction than observed for the coronary artery samples, though the NB treatment with PAS 1 gave rise to a volume reduction that was 50 % more than that for the control PAS 2.

Change in volume results for CAS 5 (NB Treated) and CAS 6 (Control) determined using IVOCT are plotted in Fig. 9 with two additional time points, 2 h and 6 h. These experiments were interrupted at three time points (2, 4, and 6 h) for plaque measurement. The measured plaque volumes indicate that the present NB treatment consistently reduced a greater volume of plaque for a given time duration compared to that for the control solution without NBs.

The present findings indicate that an AMF NB treatment uniformly led to a greater reduction of plaque volume in ex vivo artery specimens. This finding is consistent with NB induced destruction of hard tubercle deposits that contain $CaCO_3$ as a principal component [23]. By comparison, the primary mineral component found in arterial plaque is typically hydroxyapatite (HA) [31]. Given the reductions in concentration that resulted from the addition of nanobubbles indicated in Fig. 4, it appears that AMF generated nanobubbles may also bind to other nanoparticles that form in Ringer's solution and in the presence of ex

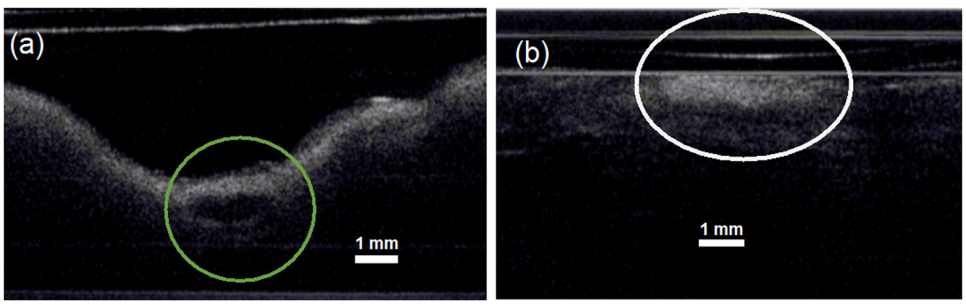

Fig. 5. IVOCT images of (a) calcified plaque CAS 3 and (b) lipid plaque CAS 2.

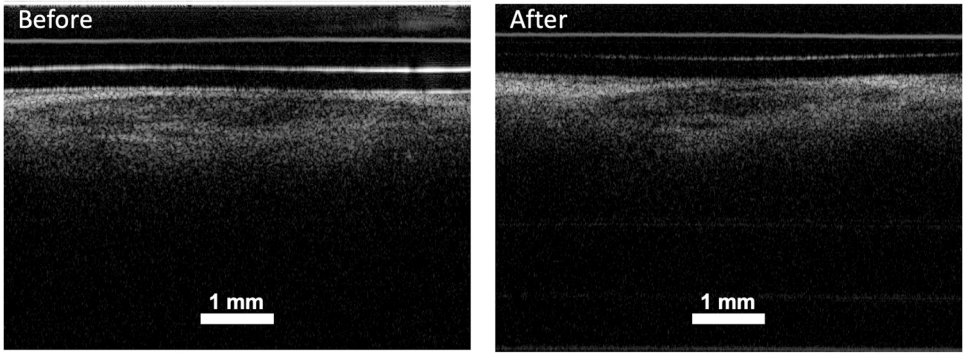

Fig. 6. Representative IVOCT images of a plaque (CAS 1 III) before and after four hours of exposure to NB treated Ringer's solution.

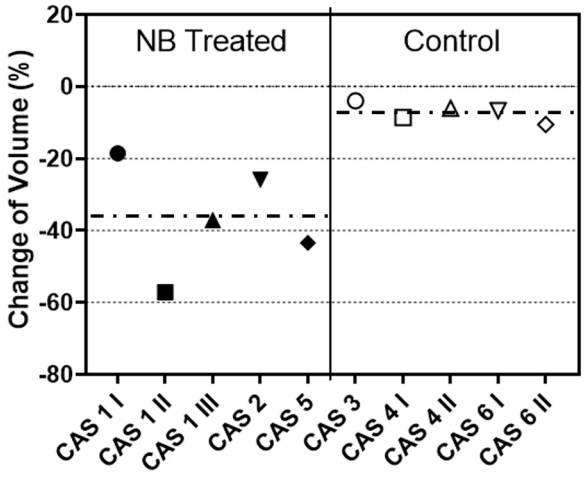

Fig. 7. Change in volume results for coronary artery samples (CAS) determined from IVOCT images. CAS 1 contained three plaques (I, II and III), CAS 4 and CAS 6 contained two plaques (I and II), and the other samples contained only one plaque. The *p* value is 0.0027 for a Student's T-test for the NB treated and control groups. The mean change in volume for each group is indicated by a dashed line.

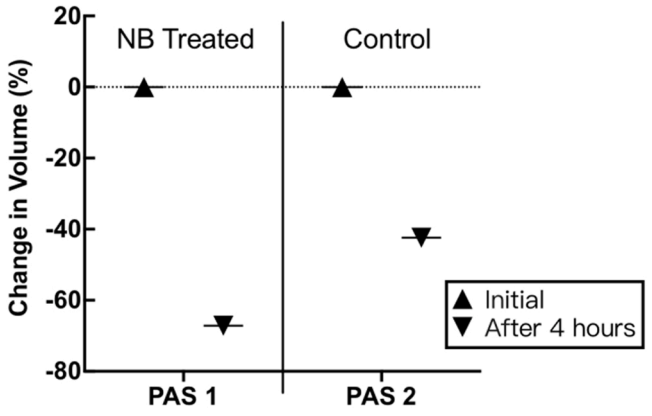

Fig. 8. Volume reduction measurements for peripheral artery samples PAS 1, which was exposed to Ringer's solution containing NBs, and PAS 2 which was a control sample exposed to unaltered Ringer's solution.

vivo tissues. This assertion is consistent with the freeze fracture TEM observations of Uchida and coworkers who showed that nanobubbles can bind to nanoparticles in both saline and wastewater [12]. Although the chemical compositions of nanoparticles in the Ringer's solution were not analyzed, it is reasonable to assume that some of them contained

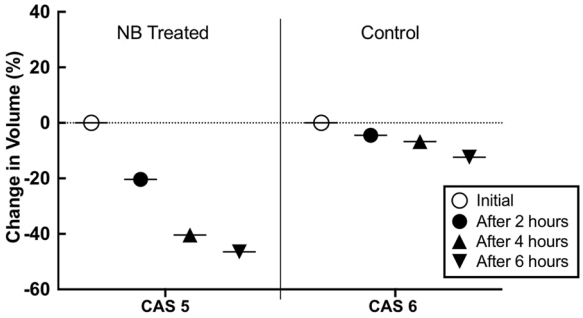

Fig. 9. IVOCT results for CAS 5 (NB treated) and CAS 6 (control) after 2, 4 and 6 h under flow conditions.

calcium, a constituent of Ringer's solution as shown in Table 1.

A reduction in volume was also measured for a lipid-type plaque that was greater than that consistently measured for plaques under control conditions, as illustrated in Fig. 7 for CAS 2. While lipid-type plaques generally contain a relatively large amount of lipid, they may not be completely devoid of HA [31]. The presence of HA in CAS 2 is evident from the dark region that can also be seen in the bottom portion of this plaque in Fig. 5(b). Although this dark area is smaller than the lighter area for this lipid type plaque, it does suggest the presence of a modest amount of HA. We note that the percent volume reduction in volume for CAS 2 was among the lowest values observed for a plaque exposed to NB treated Ringer's solution at about 25 %. This relatively low value is consistent with this lipid type plaque having a relatively low HA content compared to that for the calcified plaques.

The apparent presence of nanobubble/nanoparticle clusters with a size of about 850 nm (Fig. 4) for the test solutions supports the theory that nanobubbles can bind to unstable Ca containing embryos in solutions before they have time to completely dissolve back into solution [23]. We note that any clusters that reach a size larger than 1 μm would not be detected using NTA. Therefore, larger clusters may have been produced in the present work that were not detected. It is also not known how nanobubbles or the clusters produced may affect various parts of the human anatomy. *In vivo* animal studies are needed to determine how nanobubbles might be safely administered as well as how to optimize and improve the performance of NBs for reducing plaque in pericardial tissues.

4. Conclusion

Nanoparticle tracking analysis measurements for Ringer's solution and Ringer's solution containing NBs were found to be consistent with the assertion that nanobubbles bind to nanoparticles to form clusters in this solution and in the presence of ex vivo arterial tissues. Accordingly, we assert nanoparticles binding to nanobubbles can induce the

dissolution of in plaques, which consist of the calcium compound that is in the embryo nanoparticles clustered with NBs.

Several experiments were performed in which ex vivo human coronary artery tissues and heart valve tissues containing plaque were exposed to Ringer's solution with and without nanobubbles. *Ex vivo* measurements using IVOCT consistently indicated that plaque volume was significantly reduced in the presence of nanobubbles. The observed NB effect for reducing plaque appeared to be more distinct for coronary artery samples while the greatest reduction in plaque size was observed for the peripheral superficial femoral artery specimens. Overall, the present results indicate that there is potential for the use of nanobubbles to treat atherosclerosis.

CRediT authorship contribution statement

A. Li: Writing – original draft, Investigation, Visualization, Validation, Data curation. **Y. Li:** Investigation, Visualization. **S. Qiu:** Investigation, Visualization. **P. M. Patel:** Methodology, Writing – review & editing. **Z. Chen:** Validation, Methodology, Writing – review & editing. **J. C. Earthman:** Supervision, Conceptualization, Methodology, Data curation, Writing – review & editing.

Declaration of Competing Interest

The authors declare the following financial interests/personal relationships which may be considered as potential competing interests: James Earthman reports financial support was provided by Medtronic Inc. James C. Earthman has patent #Patent Application No. 16/160,875 pending to University of California, Irvine.

Data availability

Data will be made available on request.

Acknowledgements

The present work was supported by the Medtronic Challenge Program, Medtronic, Inc., USA (Research Agreement No. 211009). The authors thank the individuals who donated their bodies and tissues for research and the Willed Body Program at UCI for sample preparation. We also gratefully acknowledge Laser Spectroscopy Labs at UCI for use of the NanoSight NS300.

References

[1] Cardiovascular Diseases (CVDs). (n.d.). ⟨https://www.who.int/en/news-room/fact-sheets/detail/cardiovascular-diseases-(cvds)⟩. (Accessed 11 June 2021).
[2] I. Gregersen, S. Holm, T.B. Dahl, B. Halvorsen, P. Aukrust, A focus on inflammation as a major risk factor for atherosclerotic cardiovascular diseases. Expert Rev. Cardiovasc. Ther. 14 (3) (2016) 391–403.
[3] K. Kobiyama, R. Saigusa, K. Ley, Vaccination against atherosclerosis, Curr. Opin. Immunol. 59 (2019) 15–24.
[4] A. Maruf, Y. Wang, T. Yin, J. Huang, N. Wang, C. Durkan, Y. Tan, W. Wu, G. Wang, Atherosclerosis Treatment with stimuli-responsive nanoagents: recent advances and future perspectives, Adv. Healthc. Mater. (2019) 1900036.
[5] J.W.G. Tyrrell, P. Attard, Images of nanobubbles on hydrophobic surfaces and their interactions. Phys. Rev. Lett. 87 (17) (2001), 176104.
[6] F.Y. Ushikubo, T. Furukawa, R. Nakagawa, M. Enari, Y. Makino, Y. Kawagoe, T. Shiina, S. Oshita, Evidence of the existence and the stability of nano-bubbles in water. Colloids Surf. A Physicochem. Eng. Asp. 361 (1–3) (2010) 31–37.
[7] P. Attard, The stability of nanobubbles, Eur. Phys. J. Spec. Top. (2013) 1–22.
[8] F.Y. Ushikubo, M. Enari, T. Furukawa, R. Nakagawa, Y. Makino, Y. Kawagoe, S. Oshita, Zeta-potential of micro-and/or nano-bubbles in water produced by some kinds of gases, IFAC Proc. 43 (26) (2010) 283–288.
[9] P. Satpute, J.C. Earthman, Hydroxyl ion stabilization of bulk nanobubbles resulting from microbubble shrinkage, J. Colloid Interface Sci. 584 (2021) 449–455.
[10] A. Agarwal, W.J. Ng, Y. Liu, Principle and applications of microbubble and nanobubble technology for water treatment. Chemosphere 84 (9) (2011) 1175–1180.
[11] T. Temesgen, T.T. Bui, M. Han, T.I. Kim, H. Park, Micro and nanobubble technologies as a new horizon for water-treatment techniques: a review, Adv. Colloid Interface Sci. 246 (2017) 40–51.
[12] T. Uchida, S. Oshita, M. Ohmori, T. Tsuno, K. Soejima, S. Shinozaki, Y. Take, K. Mitsuda, Transmission electron microscopic observations of nanobubbles and their capture of impurities in wastewater, Nanoscale Res. Lett. 6 (1) (2011) 295.
[13] A. Ghadimkhani, W. Zhang, T. Marhaba, Ceramic membrane defouling (cleaning) by air nano bubbles, Chemosphere 146 (2016) 379–384.
[14] H. Chen, H. Mao, L. Wu, J. Zhang, Y. Dong, Z. Wu, J. Hu, Defouling and cleaning using nanobubbles on stainless steel, Biofouling 25 (4) (2009) 353–357.
[15] J. Zhu, H. An, M. Alheshibri, L. Liu, P.M. Terpstra, G. Liu, V.S. Craig, Cleaning with bulk nanobubbles, Langmuir 32 (43) (2016) 11203–11211.
[16] H. Wu, N.G. Rognin, T.M. Krupka, L. Solorio, H. Yoshiara, G. Guenette, C. Sanders, N. Kamiyama, A.A. Exner, Acoustic characterization and pharmacokinetic analyses of new nanobubble ultrasound contrast agents, Ultrasound Med. Biol. 39 (11) (2013) 2137–2146.
[17] T. Yin, P. Wang, R. Zheng, B. Zheng, D. Cheng, X. Zhang, X. Shuai, Nanobubbles for enhanced ultrasound imaging of tumors, Int. J. Nanomed. 7 (2012) 895.
[18] Y. Wang, X. Li, Y. Zhou, P. Huang, Y. Xu, Preparation of nanobubbles for ultrasound imaging and intracellular drug delivery, Int. J. Pharm. 384 (1–2) (2010) 148–153.
[19] W. Lin, X. Xie, J. Deng, H. Liu, Y. Chen, X. Fu, H. Liu, Y. Yang, Cell-penetrating peptide-doxorubicin conjugate loaded NGR-modified nanobubbles for ultrasound triggered drug delivery, J. Drug Target. 24 (2) (2016) 134–146.
[20] X. Xie, Y. Yang, W. Lin, H. Liu, H. Liu, Y. Yang, Y. Chen, X. Fu, J. Deng, Cell-penetrating peptide-siRNA conjugate loaded YSA-modified nanobubbles for ultrasound triggered siRNA delivery, Colloids Surf. B Biointerfaces 136 (2015) 641–650.
[21] H.P. Tong, L.F. Wang, Y.L. Guo, L. Li, X.Z. Fan, J. Ding, H.Y. Huang, Preparation of protamine cationic nanobubbles and experimental study of their physical properties and in vivo contrast enhancement, Ultrasound Med. Biol. 39 (11) (2013) 2147–2157.
[22] H.Y. Huang, S.H. Hu, S.Y. Hung, C.S. Chiang, H.L. Liu, T.L. Chiu, Y.Y. Chen, S. Y. Chen, SPIO nanoparticle-stabilized PAA-F127 thermosensitive nanobubbles with MR/US dual-modality imaging and HIFU-triggered drug release for magnetically guided in vivo tumor therapy, J. Control. Release 172 (1) (2013) 118–127.
[23] N.V.-Y. Quach, A. Li, J.C. Earthman, Interaction of calcium carbonate with nanobubbles produced in an alternating magnetic field, ACS J. Appl. Mater. Interfaces 12 (2020) 43714–43719.
[24] G. Bailey, J. Meadows, A.R. Morrison, Imaging atherosclerotic plaque calcification: translating biology, Curr. Atheroscler. Rep. 18 (8) (2016) 51.
[25] B. Coto, C. Martos, J.L. Peña, R. Rodríguez, G. G Pastor, Effects in the solubility of $CaCO_3$: experimental study and model description, Fluid Phase Equilib. 324 (2012) 1–7.
[26] H. Jinnouchi, Y. Sato, A. Sakamoto, A. Cornelissen, M. Mori, R. Kawakami, N. V. Gadhoke, F.D. Kolodgie, R. Virmani, A.V. Finn, Calcium deposition within coronary atherosclerotic lesion: Implications for plaque stability, Atherosclerosis 306 (2020) 85–95.
[27] M. Jonasz, G. Gournier, Light Scattering by Particles in Water: Theoretical and Experimental Foundations, Elsevier, London, 2007, p. 1.
[28] N.F. Bunkin, A.V. Shkirin, N.V. Suyazov, V.A. Babenko, A.A. Sychev, N.V. Penkov, K.N. Belosludtsev, S.V. Gudkov, Formation and dynamics of ion-stabilized gas nanobubble phase in the bulk of aqueous NaCl solutions, J. Phys. Chem. B 120 (2016) 1291–1303.
[29] C.M. Giachelli, The emerging role of phosphate in vascular calcification, Kidney Int. 75 (2009) 890–897, https://doi.org/10.1038/ki.2008.644.
[30] Y. Li, J. Jing, E. Heidari, J. Zhu, Y. Qu, Z. Chen, Intravascular optical coherence tomography for characterization of atherosclerosis with a 1.7 micron swept-source laser, Sci. Rep. 7. 1 (2017) 14525.
[31] C. Xu, J.M. Schmitt, S.G. Carlier, R. Virmani, Characterization of atherosclerosis plaques by measuring both backscattering and attenuation coefficients in optical coherence tomography, J. Biomed. Opt. 13 (3) (2008), 034003.